Supporting Information

For

Electrochemically exfoliated covalent organic frameworks for improved photocatalytic hydrogen evolution

Ting Wang [a,c,d,e,1], Ruijuan Zhang [b,1], pengda Zhai [b,*], Mingjie Li [a,d,e,*], Xinying Liu [b], Chaoxu Li [a,d,e,*]

[a] *Qingdao Institute of Bioenergy and Bioprocess Technology, Chinese Academy of Sciences, Qingdao, 266101, China*

[b] *Institute for Catalysis and Energy Solutions, University of South Africa, Private Bag X6, Florida, 1710, South Africa*

[c] *Key Laboratory of Optoelectronic Chemical Materials and Devices (Ministry of Education), School of Optoelectronic Materials & Technology, Jianghan University, 8 Sanjiaohu Road, Wuhan 430056, China*

[d] *Shandong Energy Institute, Qingdao, China*

[e] *Qingdao New Energy Shandong Laboratory, Qingdao, China*

E-mail: licx@qibebt.ac.cn, zhaipengda@163.com, limj@qibebt.ac.cn

[1] These authors contributed equally to this work.

Materials

All reagents were directly used as received from commercial sources unless otherwise noted. 5,5',5''-(benzene-1,3,5-triyl)tris(thiophene-2-carbaldehyde) (TTB-CHO), 1,3,5-Tris(4-aminophenyl)benzene (TAPB) and 2,4,6-Tris(4-aminophenyl)triazine (TAPT) were purchased from Shanghai Bide Pharmaceutical Co., Ltd or J&K scientific Co., Ltd. The Pyrex glass tubes were purchased from Synthware.

General characterization

The Fourier transform infrared spectroscopy (FT-IR) analysis was carried on PerkinElmer Spectrum 100 spectrometer. Solid-state ^{13}C NMR spectra were recorded on Bruker AVANCE III 700 MHz spectrometer. Powder X-ray diffraction (PXRD) data were collected on a Rigaku SmartLab9KW diffractometer in reflection geometry operating with a Cu Kα anode operating at 40 kV and 40 mA (2 to 50 degrees). Thermo-gravimetric analysis (TGA) was carried out on a TA Q600 TGA/DSC System analyzer under nitrogen atmosphere at a heating rate of 10 °C min^{-1} within the temperature range of 10–800 °C. Nitrogen adsorption/desorption isotherms were obtained using a Quantachrome Autosorb iQ apparatus at 77 K. The surface areas were calculated using Brunauer-Emmett-Teller (BET) methods. The X-ray photoelectron spectra (XPS) data were collected using Thermo Scientific Kα spectrometer. The scanning electron microscope (SEM) analysis was performed on a JSM-7610F scanning electron microscope (Hitachi, Tokyo, Japan). Transmission electron microscope (TEM) analysis was performed on a transmission electron microscope (JEOL, JEM-2100). The atomic force microscope (AFM) measurements were performed on a Jupiter XR AFM by Oxford Instruments. Metallographic microscope images were taken with a Lycra metallographic microscope. The contact angle data were collected using a contact angle meter of Dataphysics OCA20.

Optical and electrochemical measurements

A homogeneous slurry of COFs was prepared by dispersing 5 mg of each sample in 30 μL nafion solution in ethanol and water (v:v/1:3). Thin films of COFs were prepared by drop-coating of each sample (50 μL) on fluorine-doped tin oxide electrodes (FTO) and being dried completely.

All electrochemical tests were performed on the Versa STAT electrochemical workstation with a standard three-electrode system. The photocurrent measurements (*i-t*) were conducted under the irradiation of a 300 W Xe lamp. The electrochemical impedance (EIS) measurements were performed at the frequency range of 0.01 Hz to 100 Hz. Mott-Schottky analysis was carried out at 1000, 1500, and 2000 Hz frequency. COFs-coated FTO was used as the working electrode, Pt plate was used as the counter electrode and the Ag/AgCl electrode was used as the reference electrode, and 0.1 M Na_2SO_4 solution was used as the electrolyte.

Cyclic voltammetry (CV) was performed on the Versa STAT electrochemical workstation with a standard three-electrode system. COFs-coated FTO plate was used as the working electrode, $Ag/AgNO_3$ acetonitrile electrode was used as a reference electrode, and Pt was applied as the counter electrode, tetrabutylammonium hexafluorophosphate (0.1 M) in acetonitrile was used as the electrolyte. The potential range was set between 0 ~ 3 V or –2 ~ 0 V and the scan rate was 100 mV s^{-1}. The applied potential *vs.* Ag/AgCl was converted to Reversible Hydrogen Electrode (RHE) potentials using the following equation:

$$E_{RHE} = E_{Ag/AgCl} + 0.0591\ pH + E^{\theta}_{Ag/AgCl}\ (E^{\theta}_{Ag/AgCl} = 0.197\ V)$$

The UV-Vis adsorption spectra of the polymers were obtained for the dry-pressed disk samples on a Scan UV-Vis spectrophotometer (UV-Lambda 950, PerkinElmer, US) using $BaSO_4$ as a reference sample. The fluorescence properties of the materials were measured with a Shimadzu F-7000 PC fluorescence spectrometer by using excitation wavelength of 380 nm at room temperature. The fluorescence decay curves were performed on Edinburgh Instruments FLS 920 fluorescence spectrometer. Temperature-dependent photoluminescence (PL) spectra from 100 to 298 K were recorded on Edinburgh Instruments FLS1000 spectrophotometer.

Photocatalytic H_2 evolution experiments

The photocatalytic experiments were conducted with a 300 W Xe lamp (Beijing PerfectLight Technology Co., Ltd). The reaction system temperature was maintained at 5 °C by a flow of cooling water. Before irradiation, the reaction system was carefully evacuated to remove air. The high purity argon was used as the carrier gas.

For photocatalytic hydrogen evolution half reaction, a certain amount of photocatalyst was dispersed into 100 mL solvent (H_2O : DMF = 83 mL : 17 mL), ascorbic acid as a sacrificial agent, and Pt as the co-catalyst. The evolved gas was analyzed using a gas chromatograph equipped with a 5 Å molecular sieve column at 120 °C with argon as carrier gas. Hydrogen was detected using a thermal conductivity detector (TCD) referenced against standard gas with a known concentration of hydrogen.

Apparent quantum efficiency (AQE)

The AQE for hydrogen was measured under the irradiation of a Xenon lamp equipped with different bandpass filter (475 nm), followed by using the equation:

$$AQE = \frac{N_e}{N_p} \times 100\% = \frac{2 \times M \times N_A}{\frac{E_{total}}{E_{photo}}} \times 100\% = \frac{2 \times M \times N_A}{\frac{P \times S \times t}{h \times c/\lambda}} \times 100\% = \frac{2 \times M \times N_A \times h \times c}{P \times S \times t \times \lambda} \times 100\%$$

Where M is the amount of H_2 (mol), N_A is Avogadro constant (6.02×10^{23} mol^{-1}), h is the Planck constant (6.626×10^{-34} J s), c is the speed of light (3×10^{8} m s^{-1}), S is the irradiation area (cm^2), P is the intensity of irradiation light (W cm^{-2}), t is the photoreaction time (s), λ is the wavelength of the monochromatic light (m).

Computational details

The HOMO-LUMO orbitals, surface electrostatic potentials and electron density differences were calculated using the Gaussian 09W program. During geometry and frequency optimization, all atoms were allowed to move freely. Based on the Density Functional Theory (DFT), the orbitals calculation was carried out using the B3LYP/6-31G (d, p) basis set.

Synthetic procedures

Synthetic routes of TTB-PB: Based on the typical COF synthesis procedure, 5,5',5''-(benzene-1,3,5-triyl)tris(thiophene-2-carbaldehyde) (TTB-CHO) (12.25 mg, 0.03 mmol), 1,3,5-Tris(4-aminophenyl)benzene (TAPB) (10.54 mg, 0.03 mmol) and *o*-dichlorobenzene/*n*-butyl alcohol (0.1:1.9 v/v, 2 mL) were added to a 10 mL Pyrex tube. After the mixture was sonicated for 1 min, uniform yellow suspension was formed. Subsequently, 0.1 mL of acetic acid (6 M) was added. After sonicated for

another 1 min, the tube was degassed by at least three “freeze-pump-thaw” cycles at 77 K using a liquid N_2 bath. After that, the tube was sealed under vacuum and then heated at 120 °C for 3 days. A yellow precipitate was obtained, which was collected by sucking filtration and thoroughly washed with *N*, *N*-dimethylformamide, tetrahydrofuran, and acetone, respectively. The collected sample was dried under vacuum overnight to give yellow powder (83% yield).

Synthetic routes of TTB-PT: Analogously, 5,5',5''-(benzene-1,3,5-triyl)-tris(thiophene-2-carbaldehyde) (TTB-CHO) (12.25 mg, 0.03 mmol), 2,4,6-Tris(4-aminophenyl)triazine (TAPT) (10.63 mg, 0.03 mmol) and *o*-dichlorobenzene/*n*-butyl alcohol (0.1:1.9 v/v, 2 mL) were used to synthesize TTB-PT. An orange powder was obtained (72% yield).

Synthetic routes of Exfo-TTB-PB and Exfo-TTB-PT: The delamination process was performed using a two-electrode system. Briefly, crystalline TTB-COFs powders (20 mg) were loaded on the foam nickel, which was used as cathodes, while platinum was used as the anodes. The electrodes were immersed into tetrabutylammonium hydrogen sulfate (TBAHS) aqueous solution (0.1 M), following with an electrochemical voltage of 5 V. After complete delamination, exfoliated COFs dispersion was quickly transferred into a centrifuge tube and centrifuged at 3000 rpm for 5 min to remove the unexfoliated and thick-layered flakes. Then the supernatants were separated for further characterization.

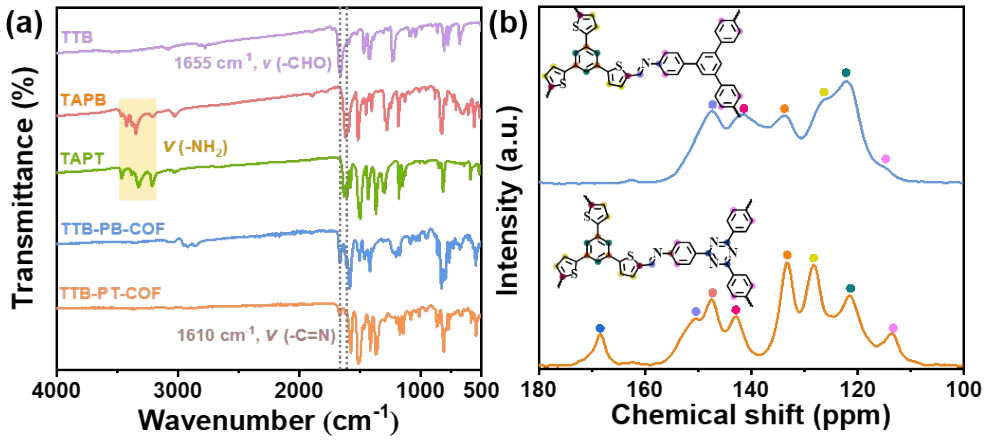

Figure S1. (a) FT-IR spectra of TTB-COFs and corresponding precursors. (b) Solid-state ^{13}C NMR spectra of TTB-COFs.

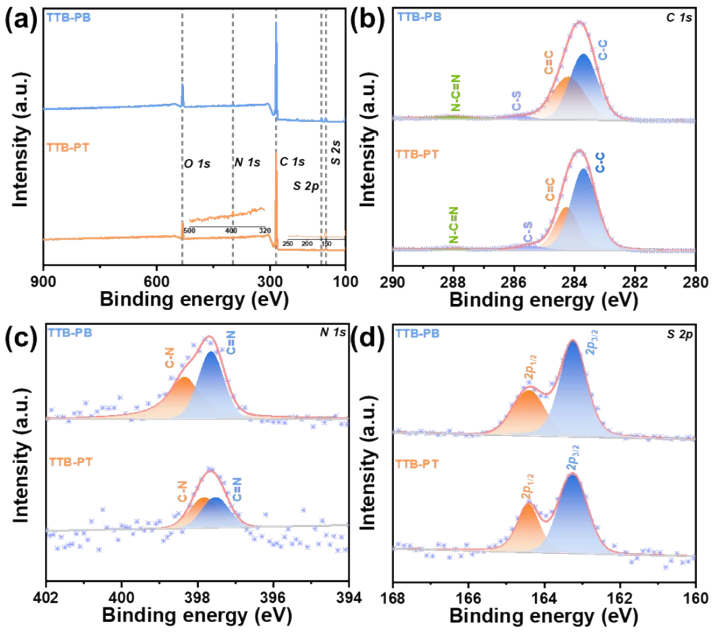

Figure S2. (a) Wide scan survey, and (b-d) high-resolution C1s (b), N1s (c), and S2p (d) XPS spectra of TTB-PB and TTB-PT.

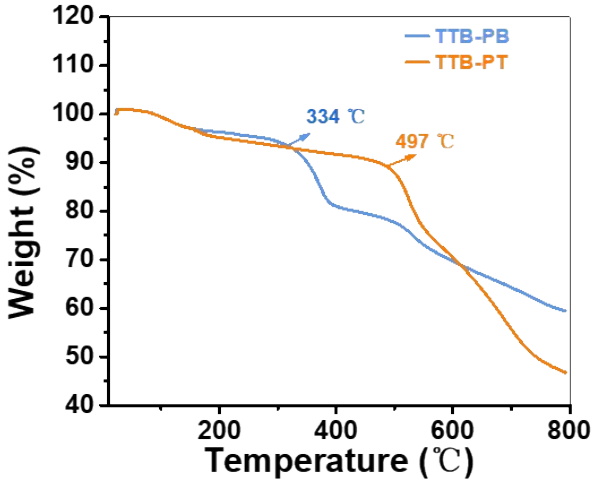

Figure S3. TGA curves of TTB-PB and TTB-PT.

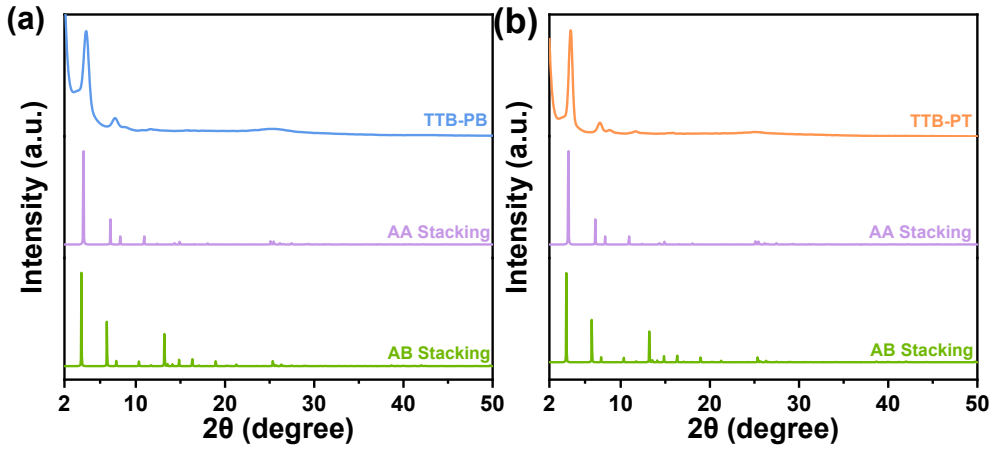

Figure S4. Comparison of experimental and simulated PXRD patterns (AA stacking and AB stacking) for (a) TTB-PB and (b) TTB-PT.

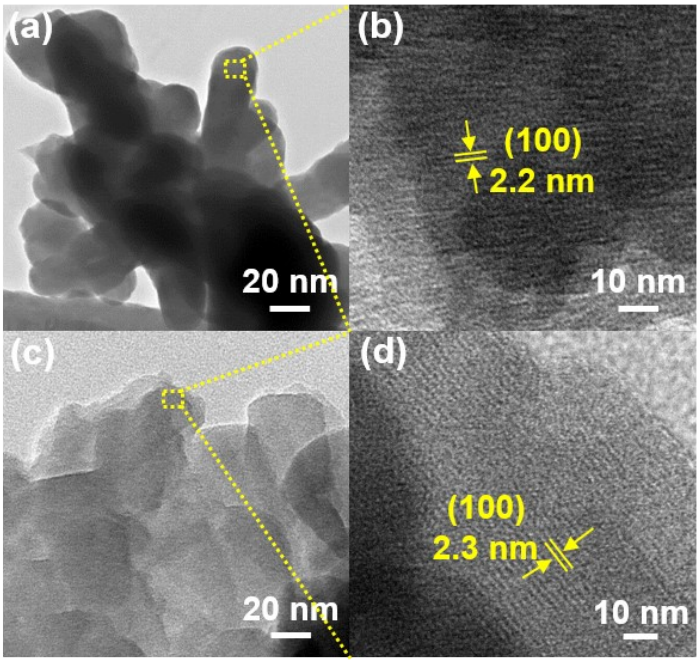

Figure S5. TEM images for (a, b) TTB-PB and (c, d) TTB-PT.

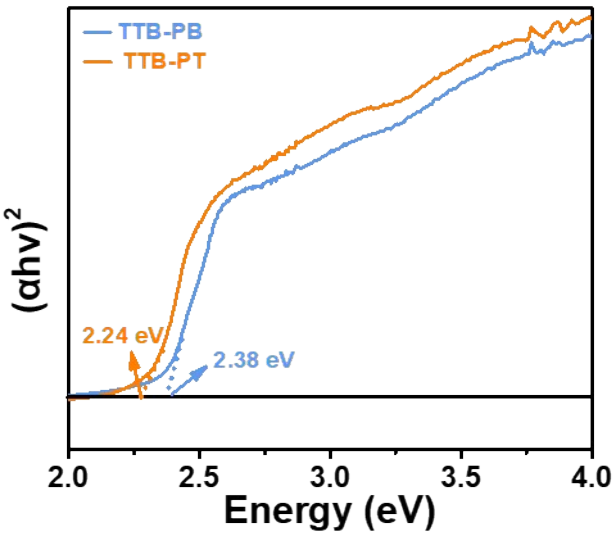

Figure S6. Comparison of Tauc plots of TTB-PB and TTB-PT.

According to the Kubelka-Munk function: $(F(R)=K/S=(1-R_\infty)^2/2R_\infty$ (K is the absorption coefficient, S is the scattering coefficient, and R_∞ is the limitation of reflection coefficient) and Tauc plot: $(\alpha h\upsilon)^n = A(h\upsilon - E_g)$, the Tauc equation can be changed into: $[F(R)h\upsilon]^n = A(h\upsilon - E_g)$. Here, n is 1/2 for indirect band gap semiconductors; For direct band gap semiconductor, n is 2. Therefore, both TTB-PB and TTB-PT are direct band gap semiconductors (n=2).

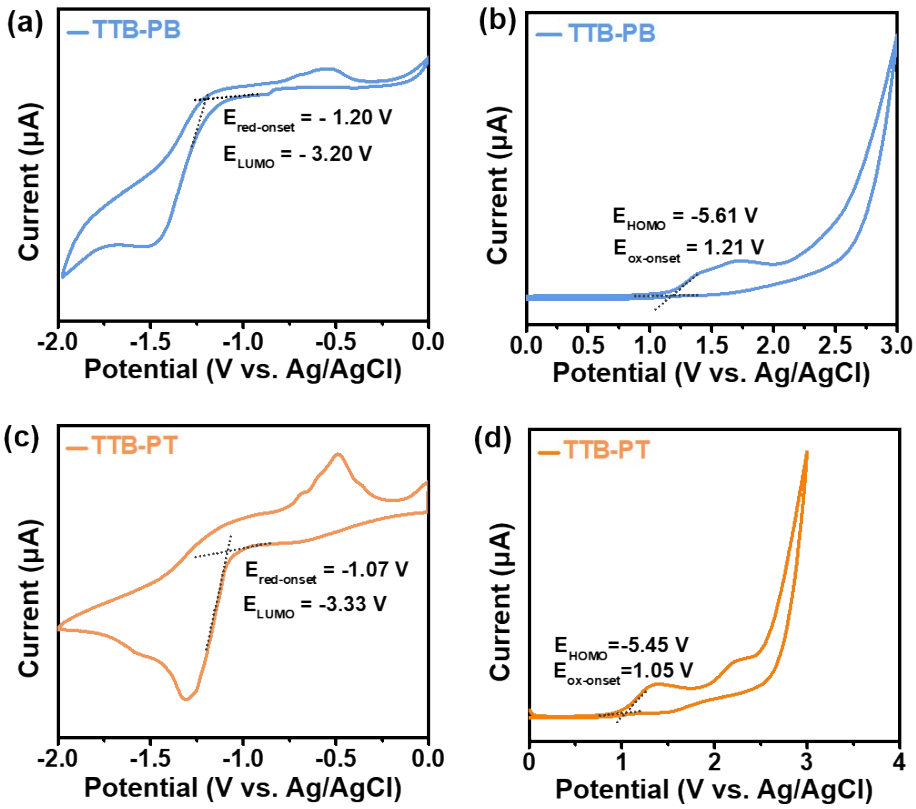

Figure S7. The CV measurements of (a, b) TTB-PB and (c, d) TTB-PT in acetonitrile solution using tetrabutylammonium hexafluorophosphate (0.05 M) as supporting electrolyte. The E_{LUMO} is calculated by the empirical formulate: $E_{LUMO} = -(E_{red\text{-}onset} + 4.4)$ eV, $E_{HOMO} = -(E_{ox\text{-}onset} + 4.4)$ eV.

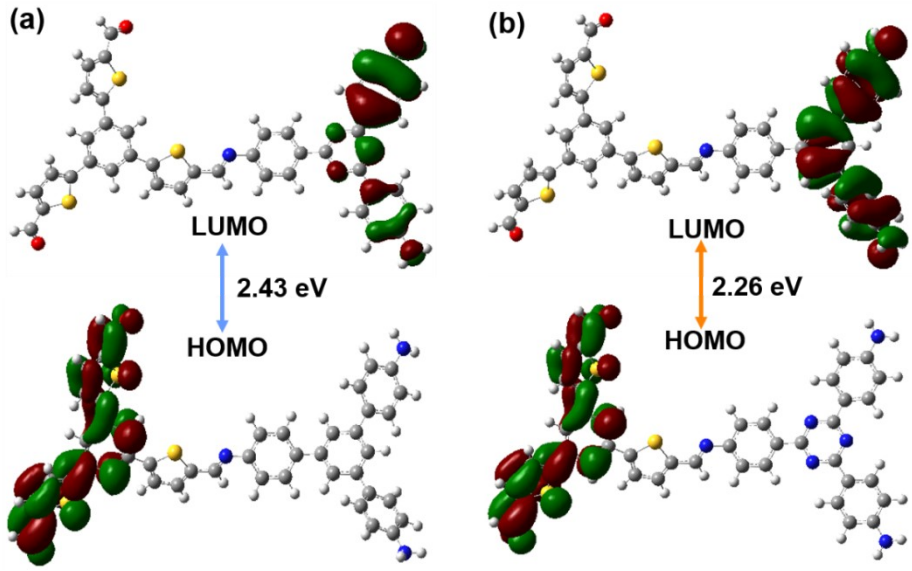

Figure S8. Frontier molecular orbital pictures and their energies of (a) TTB-PB and (b) TTB-PT.

Table S1. Energy levels and band gaps (E_g) obtained from electrochemical (E_g^{elec}), optical (E_g^{opt}), and simulated (E_g^{cal}) method

	TTB-PB			TTB-PT		
(eV)	E_g^{elec}	E_g^{opt}	E_g^{cal}	E_g^{elec}	E_g^{opt}	E_g^{cal}
LUMO	–3.20	–	–2.70	–3.33	–	–3.22
HOMO	–5.61	–	–5.13	–5.45	–	–5.48
E_g	2.41	2.38	2.43	2.12	2.24	2.26

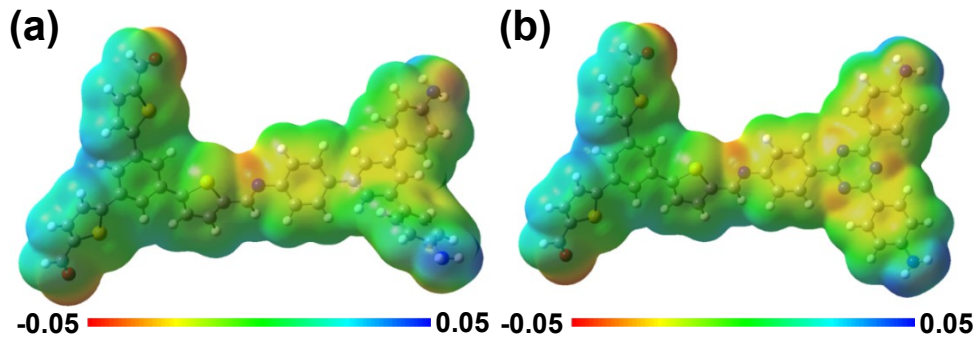

Figure S9. Electrostatic surface potentials (ESPs) distributions of the minimum repeating building blocks for (a) TTB-PB and (b) TTB-PT using DFT at the B3LYP/6-31G(d) level.

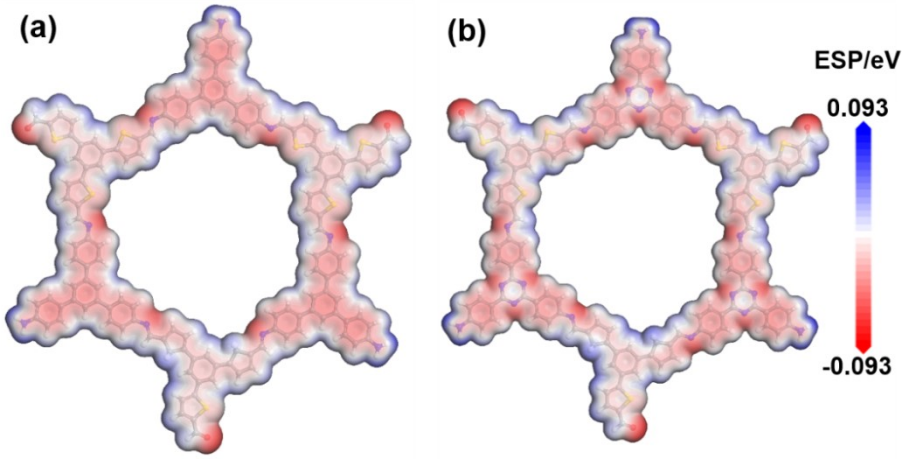

Figure S10. ESPs distributions of single hexagonal cell for (a) TTB-PB and (b) TTB-PT using DFT at the B3LYP/6-31G (d) level.

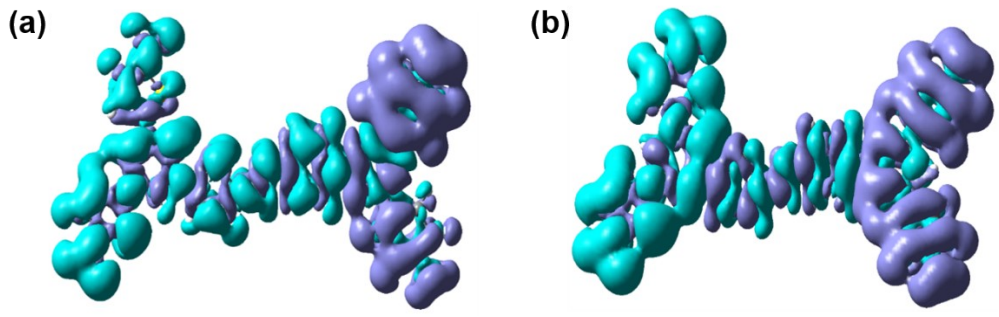

Figure S11. The calculated charge density difference of (a) TTB-PB and (b) TTB-PT in the excited state. Blue and purple represented electron accumulation and depletion, respectively.

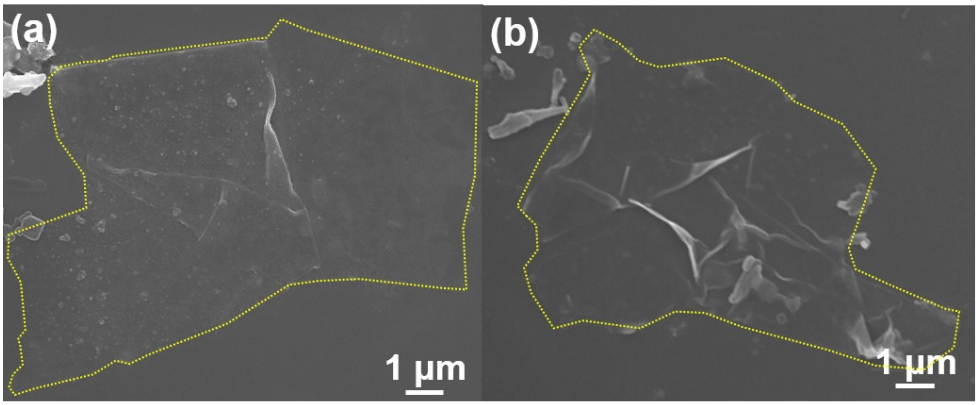

Figure S12. SEM images of (a) Exfo-TTB-PB and (b) Exfo-TTB-PT.

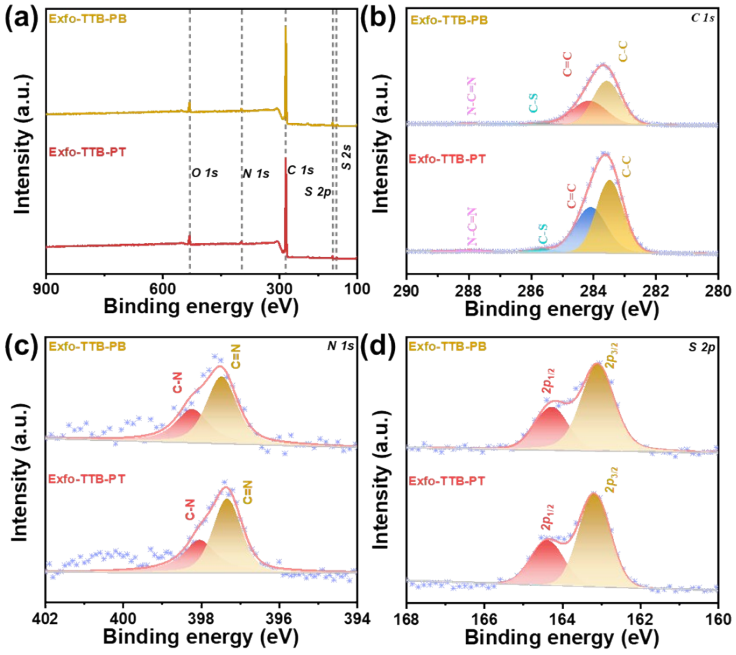

Figure S13. (a) Wide scan survey, and (b-d) high-resolution C1s (b), N1s (c), and S2p (d) XPS spectra of Exfo-TTB-PB and Exfo-TTB-PT.

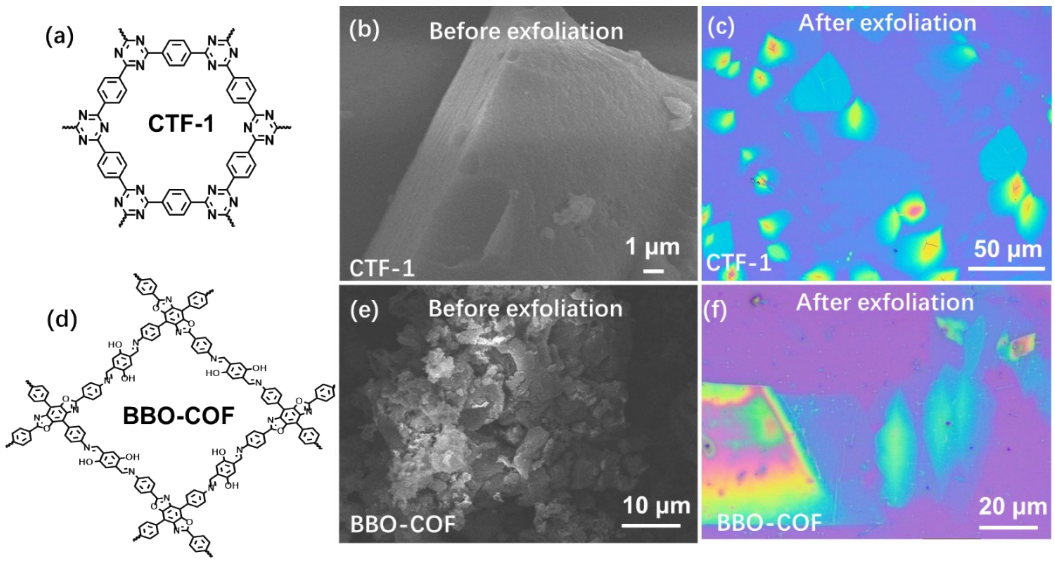

Figure S14. (a & d) The chemical structures of CTF-1(a) and BBO-COF (d). (b) & (e) SEM images of CTF-1(b) and BBO-COF (e) before electrochemical exfoliation. (c) & (f) Metallographic microscope images of CTF-1(c) and BBO-COF (f) after electrochemical exfoliation.

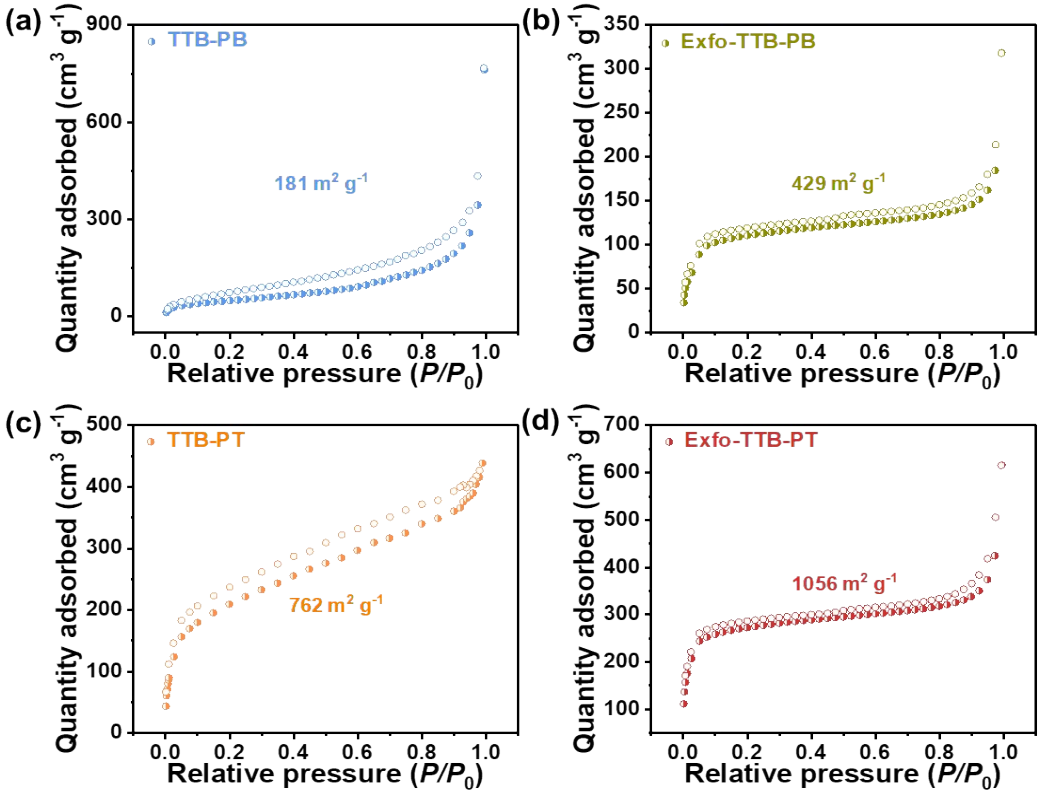

Figure S15. N_2 adsorption-desorption isotherms of TTB-PB, TTB-PT, Exfo-TTB-PB and Exfo-TTB-PT.

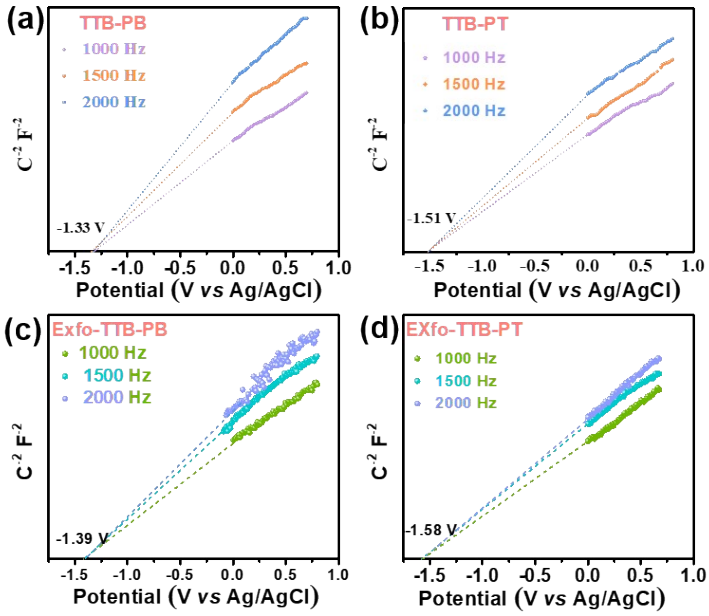

Figure S16. The MS measurements of (a) pristine bulk TTB-PB, (b) Exfo-TTB-PB, c) pristine bulk TTB-PT, and (d) Exfo-TTB-PT.

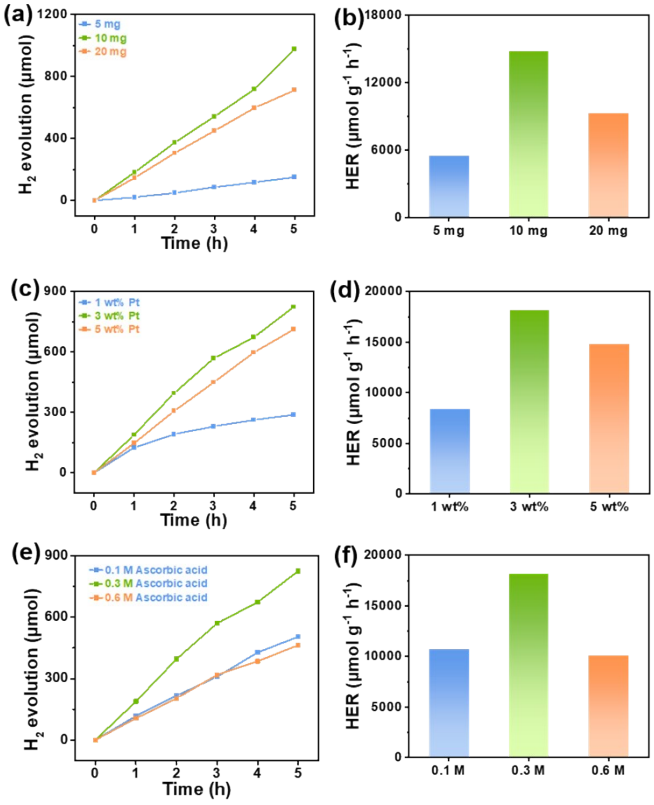

Figure S17. Time-dependent H_2 evolution (a, c, e) and H_2 evolution rate (b, d, f) of TTB-PT by varying (a, b) catalyst amount, (c, d) Pt dosage, and (e, f) sacrificial reagent concentration.

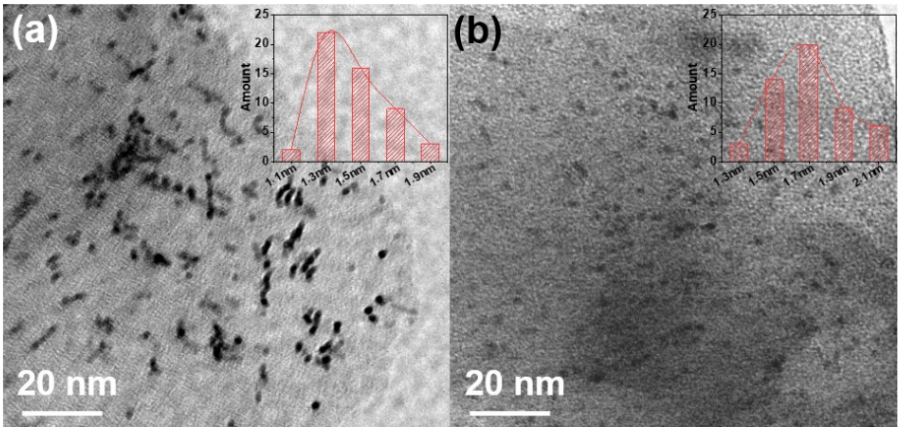

Figure S18. TEM images for bulk COFs after the photocatalysis experiments: (a) TTB-PB and (b) TTB-PT.

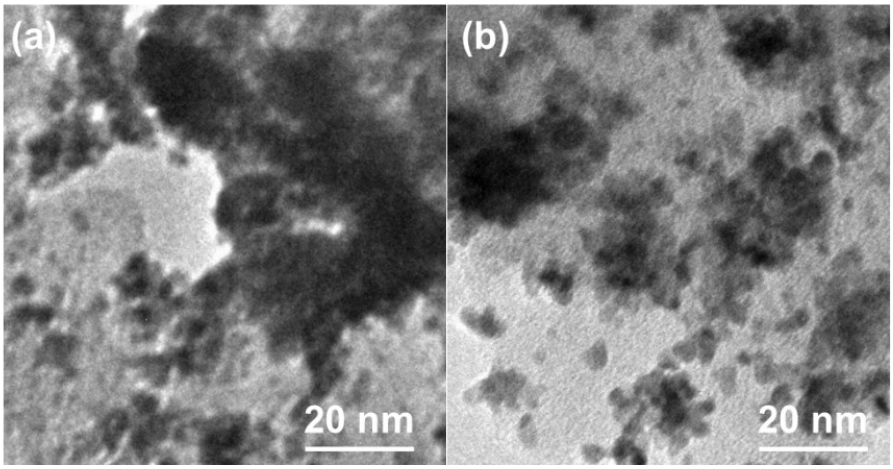

Figure S19. TEM images of (a) Exfo-TTB-PB and (b) Exfo-TTB-PT with Pt deposition after photocatalysis.

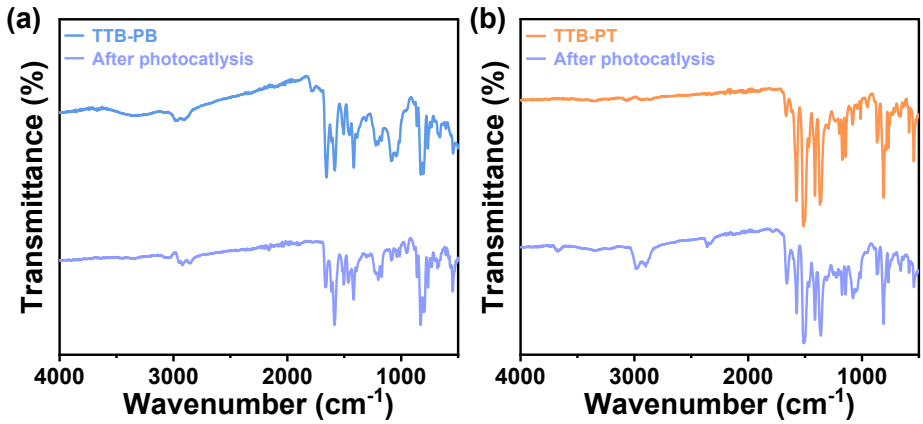

Figure S20. FT-IR spectra of (a) TTB-PB and (b) TTB-PT before and after photocatalysis.

Table S2. Comparison of photocatalytic HER performance of thiophen-based COFs photocatalysts.

Photocatalysts (amount)	Linkage	Cocatalyst	Irradiation condition	Sacrificial reagent	HER mmol h^{-1} g^{-1}	AQE (%)	Reference
TThB-TZ-COF (5 mg)	**Imine**	8 wt% Pt	300 W Xe lamp λ > 420 nm	0.1 M AA	1.03	-	*ACS Appl. Mater. Interfaces* 2023, 15, 16794−16800
BTTh-TZ-COF (5 mg)	**Imine**	8 wt% Pt	300 W Xe lamp λ > 420 nm	0.1 M AA	5.22	-	
COF-JLU36 (10 mg)	**Imine**	1 wt% Pt	300 W Xe lamp λ > 420 nm	0.1 M AA	14.6	0.37 (450 nm)	*J. Am. Chem. Soc.* 2023, 145, 8364−8374
S-COF (5 mg)	**Keto-enamine**	1 wt% Pt	300 W Xe lamp λ > 420 nm	0.01 M AA	16.3	-	*Nat. Chem.* **2022**, 13, 1180.
BTT-BPy-COF (3 mg)	**Vinylene**	3.8 wt% Pt	300 W Xe lamp λ > 420 nm	0.1 M AA	15.8	2.06 (500 nm)	*Angew. Chem. Int. Ed.* **2023**, 62, e202300224.
CTF-BT/Th-1 (3 mg)	**Triazine**	3 wt% Pt	300 W Xe lamp λ > 420 nm	0.1 M AA	6.6	7.3 (420 nm)	*Angew. Chem. Int. Ed.* **2019**, 58, 8676–8680.
TTB-PB (10mg)	**Imine**	3 wt% Pt	300 W Xe lamp λ > 420 nm	0.3 M AA	4.15	0.96 (475 nm)	***This work***
Exo-TTB-PB (10mg)	**Imine**	3 wt% Pt	300 W Xe lamp λ > 420 nm	0.3 M AA	9.86	1.25 (475 nm)	
TTB-PT (10mg)	**Imine**	3 wt% Pt	300 W Xe lamp λ > 420 nm	0.3 M AA	**18.26**	2.21 (475 nm)	
Exo-TTB-PB (10mg)	**Imine**	3 wt% Pt	300 W Xe lamp λ > 420 nm	0.3 M AA	**27.24**	3.53 (475 nm)	

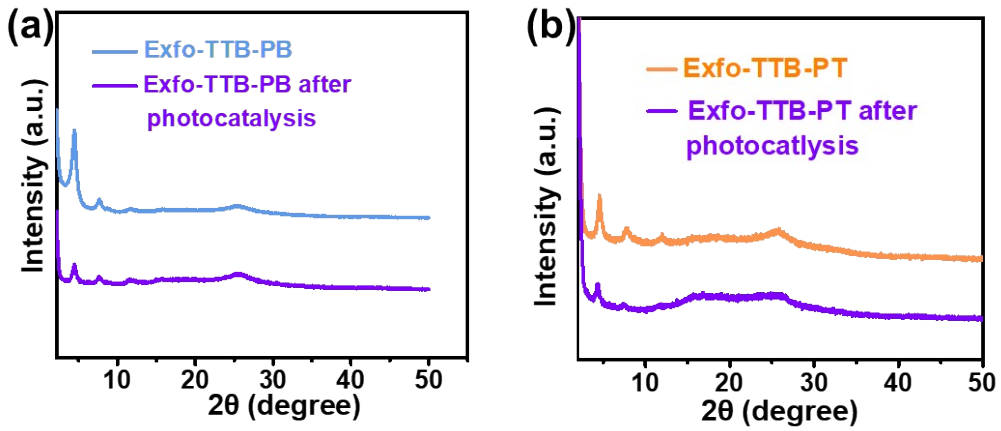

Figure S21. PXRD spectra of (a) Exfo-TTB-PB and (b) Exfo-TTB-PT before and after photocatalysis.